2009-12

# Dynamic loading characteristics in metals and composites

Tan, Kian Sing.

Monterey, California. Naval Postgraduate School


# NAVAL POSTGRADUATE SCHOOL

**MONTEREY, CALIFORNIA**

# THESIS

**DYNAMIC LOADING CHARACTERISTICS IN METALS AND COMPOSITES**

by

Tan, Kian Sing

December 2009

| | |
|---|---|
| Thesis Advisor: | Kwon, Young |
| Second Reader: | Didoszak, Jarema |

**Approved for public release; distribution is unlimited**

THIS PAGE INTENTIONALLY LEFT BLANK

| REPORT DOCUMENTATION PAGE | | | *Form Approved OMB No. 0704-0188* |
|---|---|---|---|
| Public reporting burden for this collection of information is estimated to average 1 hour per response, including the time for reviewing instruction, searching existing data sources, gathering and maintaining the data needed, and completing and reviewing the collection of information. Send comments regarding this burden estimate or any other aspect of this collection of information, including suggestions for reducing this burden, to Washington headquarters Services, Directorate for Information Operations and Reports, 1215 Jefferson Davis Highway, Suite 1204, Arlington, VA 22202-4302, and to the Office of Management and Budget, Paperwork Reduction Project (0704-0188) Washington DC 20503. | | | |
| **1. AGENCY USE ONLY** ***(Leave blank)*** | **2. REPORT DATE** December 2009 | **3. REPORT TYPE AND DATES COVERED** Master's Thesis | |
| **4. TITLE AND SUBTITLE** Dynamic Loading Characteristics in Metals and Composites | | **5. FUNDING NUMBERS** | |
| **6. AUTHOR(S)** Tan, Kian Sing | | | |
| **7. PERFORMING ORGANIZATION NAME(S) AND ADDRESS(ES)** Naval Postgraduate School Monterey, CA 93943-5000 | | **8. PERFORMING ORGANIZATION REPORT NUMBER** | |
| **9. SPONSORING /MONITORING AGENCY NAME(S) AND ADDRESS(ES)** N/A | | **10. SPONSORING/MONITORING AGENCY REPORT NUMBER** | |
| **11. SUPPLEMENTARY NOTES** The views expressed in this thesis are those of the author and do not reflect the official policy or position of the Department of Defense or the U.S. Government. | | | |
| **12a. DISTRIBUTION / AVAILABILITY STATEMENT** Approved for public release; distribution is unlimited | | **12b. DISTRIBUTION CODE** | |


**13. ABSTRACT (maximum 200 words)**

This study investigates the mechanical characteristics of aluminum alloy AA3003-H14 when it is subjected to dynamic axial loads at low strain rates of less than 1 $s^{-1}$. The tensile experiments show that both the ultimate and yield stresses, as well as the absorbed strain energy, increase with strain rate. Moreover, the strains at yield, ultimate load and fracture show positive sensitivity to strain rate. On the other hand, when the material is subjected to dynamic loading rates of more than $10^{-1}$ $s^{-1}$, the elastic modulus diminishes as the strain rate increases, while both normalized yield and ultimate stresses increase noticeably. It is also appreciated that the amount of plastic strain energy accumulated in a ductile material in its loading time history is useful as a failure criterion for the prediction of failure. Finally, a failure criterion is proposed for loading with varying strain rates.


| **14. SUBJECT TERMS** Tensile tests, strain rate effects, dynamic loading, failure criterion | | | **15. NUMBER OF PAGES** 55 |
|---|---|---|---|
| | | | **16. PRICE CODE** |
| **17. SECURITY CLASSIFICATION OF REPORT** Unclassified | **18. SECURITY CLASSIFICATION OF THIS PAGE** Unclassified | **19. SECURITY CLASSIFICATION OF ABSTRACT** Unclassified | **20. LIMITATION OF ABSTRACT** UU |

NSN 7540-01-280-5500 Standard Form 298 (Rev. 2-89)
Prescribed by ANSI Std. 239-18

THIS PAGE INTENTIONALLY LEFT BLANK

**Approved for public release; distribution is unlimited**

# DYNAMIC LOADING CHARACTERISTICS IN METALS AND COMPOSITES

Kian Sing Tan
B. Eng, National University of Singapore, 2003

Submitted in partial fulfillment of the
requirements for the degree of

**MASTER OF SCIENCE IN MECHANICAL ENGINEERING**

from the

**NAVAL POSTGRADUATE SCHOOL**
**December 2009**

Author: Kian Sing Tan

Approved by: Young Kwon
Thesis Advisor

Jarema Didoszak
Second Reader

Knox T. Millsaps, PhD
Chairman, Department of Mechanical and Astronautical Engineering

THIS PAGE INTENTIONALLY LEFT BLANK

# ABSTRACT

This study investigates the mechanical characteristics of aluminum alloy AA3003-H14 when it is subjected to dynamic axial loads at low strain rates of less than 1 $s^{-1}$. The tensile experiments show that both the ultimate and yield stresses, as well as the absorbed strain energy, increase with strain rate. Moreover, the strains at yield, ultimate load and fracture show positive sensitivity to strain rate. On the other hand, when the material is subjected to dynamic loading rates of more than $10^{-1}$ $s^{-1}$, the elastic modulus diminishes as the strain rate increases, while both normalized yield and ultimate stresses increase noticeably. It is also appreciated that the amount of plastic strain energy accumulated in a ductile material in its loading time history is useful as a failure criterion for the prediction of failure. Finally, a failure criterion is proposed for loading with varying strain rates.

THIS PAGE INTENTIONALLY LEFT BLANK

# TABLE OF CONTENTS

THIS PAGE INTENTIONALLY LEFT BLANK

# LIST OF FIGURES

THIS PAGE INTENTIONALLY LEFT BLANK

# LIST OF TABLES

THIS PAGE INTENTIONALLY LEFT BLANK

# ACKNOWLEDGMENTS

I would like to thank Professor Young Kwon for his guidance throughout the course of this thesis work and for making the process an enjoyable one. In addition, this thesis would not have been possible without Professor Jarema Didoszak. I am also grateful to Dr. Park Chanman for explaining the operation of the tensile machine, and to Mr. John Mobley who assisted in the fabrication of my specimens. I would also like to express appreciation to Lt. Angela Owens who patiently demonstrated the procedures for composite fabrication.

THIS PAGE INTENTIONALLY LEFT BLANK

# I. INTRODUCTION

The behavior of materials under high rates of strain may be vastly differently from that under static loading conditions. As the strain rate increases, the failure mode may change and the material strength may vary. This behavior, which differs for different materials, remains to be thoroughly investigated and appreciated. While the static strengths of composite materials, for example, have been considerably explored and documented, fewer studies have investigated their performance under dynamic loadings.

Research on the effect of strain rate on the strength of materials is important to the design of their applications. An unmanned aerial vehicle, for example, may experience significantly higher loads only during the launch and recovery phases of their flights. Since these are not sustained static loads, the design of such vehicles to meet strength requirements derived from treating these loads under static conditions may be excessively conservative. Higher weights result and performance specifications are thus lowered.

## A. LITERATURE REVIEW

### 1. Dynamic Loading on Metals

Hadianfard *et al.* [1] investigated the effect of the rate of strain on the mechanical properties and failure mechanisms of the aluminum alloys, AA5754 and AA5182. Conducting quasi-static tensile tests at strain rates of less than $10^{-1}$ $s^{-1}$, their results indicated negative strain rate sensitivity in these alloys. Both ultimate and yield strengths were reduced as the strain rate was increased. Moreover, the flow stresses and the strains to failure tended to decrease with higher quasi-static strain rates. The serrated yielding phenomenon associated with the nucleation and propagation of deformation band along the tensile specimen was observed. On the other hand, at dynamic rates of strain, the studied alloys exhibited mild positive sensitivity. The elongation to failure increased with the strain rate.

Accordingly, different failure mechanisms were also observed in the quasi-static and dynamic tensile tests. Under quasi-static conditions, strain localization and shear band formation were found to be necessary pre-requisites for damage and final failure to occur. The thickness of the shear bands, as well as the average size of the damaged particles, was observed to increase with increasing strain rates. The contrary was true under dynamic conditions. The void nucleation, growth and coalescence process at the second phase particles was the dominant failure mechanism under dynamic conditions. Shear banding was less pronounced.

Hadianfard *et al.* attributed the negative strain rate sensitivity in the quasi-static tensile tests to the dynamic strain ageing phenomenon which was manifested in the serrations. Being diffusion controlled, dynamic strain ageing was influenced by temperature and strain rate. Higher flow stresses at very low strain rates were the consequence of solute atoms interacting with obstacles preventing dislocation movements. With increasing strain rate, this dampening effect was thus reduced and lower flow stresses resulted.

Similar results were also obtained by Mukai *et al.* [2] in fine-grained IN905XL aluminum alloys when they examined the dependence of their mechanical properties on the rate of deformation. When dealing with up to a strain rate of 10 $s^{-1}$, all samples showed negative strain rate sensitivity of flow stress. Positive strain rate sensitivity of strength was, however, observed above strain rates of $10^3$ $s^{-1}$. In addition, while yield stress and total elongation were weak functions of the strain rate below a strain rate of $10^{-1}$ $s^{-1}$, both increased significantly with higher strain rates when the strain rate exceeded $10^3$ $s^{-1}$.

In their tensile experiments on the aluminum alloy 6061, Srivatsan *et al.* [3] varied the strain rate from $10^{-4}$ $s^{-1}$ to $10^{-1}$ $s^{-1}$. Likewise, they observed negative strain rate sensitivity, with yield and ultimate strengths diminishing as strain rate increased. Concomitantly, both the elongation to failure and the reduction in area increased. These observations were the result of shorter test times at high strain rates. Hence, interactions between dislocations and the primary hardening precipitates ($Mg_2Si$) and interactions between dislocations and the coarse constituent particles were limited. The material

strength was thus lower and this, together with fewer micro-cracks due to reduced interactions between dislocations and inter-metallic particles, resulted in enhancements in the elongation to failure.

Yu and Jones [4] conducted tensile tests on both aluminum alloy and mild steel specimens. They carried out quasi-static experiments at strain rates of less than 2 x $10^{-2}$ $s^{-1}$ and dynamic tests up to a maximum strain rate of 140 $s^{-1}$. Their observations showed that the flow stress of aluminum alloy was insensitive to the rate of deformation. The latter affected only the rupture conditions, augmenting both the engineering and true rupture strains with increasing strain rate.

Results on the mild steel specimens indicated that strain rate had a weaker effect on mild steel at large plastic strains than at small plastic strains. In addition, although the true rupture strain was nearly unaffected by strain rate, the true rupture stress increased about 20% when the strain rate was increased from $10^{-3}$ $s^{-1}$ to $10^{2}$ $s^{-1}$. Good agreement was found when the Cowper-Symonds constitutive equation which is reproduced as Equation (1), was fitted to the experimental data.

$$\sigma = \sigma_0(\varepsilon)[1 + \frac{\dot{\varepsilon}}{D}]^{\frac{1}{p}} \qquad (1)$$

$\sigma_0(\varepsilon)$ refers to the static stress-strain relation while D and p are material constants.

The dynamic uniaxial stress-strain relationship was also studied by Albertini and Montagnani [5] in austenitic stainless steels. Ranging the strain rate between $10^{-2}$ $s^{-1}$ and 5 x $10^{2}$ $s^{-1}$, they found that higher strain rates led to increasing flow stresses but decreasing uniform and fracture elongations.

## 2. Dynamic Loading on Composites

Armenakas and Sciammarella [6] reported experimental findings on the mechanical properties of glass fiber reinforced epoxy plates subjected to high rates of

strain in the direction of the fibers. Analyzing their results, they established that the dynamic elastic modulus varies linearly with the logarithm of the strain rate.

Dynamic loading tensile tests were also performed by Lifshitz [7] on balanced angle ply glass fiber reinforced epoxy composites. Failure stresses were observed to be considerably higher than the corresponding static values whereas failure strains and moduli were insensitive to the rate of loading.

Daniel *et al.* [8] tested and characterized unidirectional graphite/epoxy laminates in the form of thin ring specimens at high strain rates. The dynamic modulus exceeded the static modulus by approximately 20 percent while the dynamic strength and ultimate strain were close to the static properties.

Applying a novel technique to the tensile impact testing of both uniaxially reinforced carbon fiber/epoxy and woven-roving reinforced glass fiber/epoxy composites, Harding and Welsh [9] showed that the modulus, the fracture strength and the failure mode of the carbon fiber/epoxy composite were dependent of the strain rate. In contrast, impact rates of strain lead to significant increases in the failure strength, the failure strain, the absorbed failure energy and the modulus of the glass fiber/epoxy composite. Unlike the carbon fiber/epoxy composite in which damage was confined to areas near the fracture plane, damage in the glass fiber/epoxy composite extended over the gauge region with increasing strain rates. Extensive debonding also occurred between the fibers and the matrix.

In their literature survey on dynamically loaded composites, Melin and Asp [10] noted the difficulty in comparing results from various investigations since the assessed strain-rate dependencies were prone to influence from variations in fiber volume fractions and materials. Their research investigated the effects of the strain rate on the transverse tension properties of a carbon fibers/epoxy composite. By varying the strain rate between 100 and 800 $s^{-1}$, they found weak or no dependence of the transverse mechanical properties on the strain rate.

Through tensile tests performed on glass/epoxy laminates at over a range of strain rates, Okoli and Smith [11] demonstrated that the Poisson's ratio is insensitive to the

strain rate. This could be attributed to the presence of fibers in the composites. They also commented that the Eyring theory of viscosity described the strain rate effects on most unfilled polymers. The theory assumed that the deformation of a polymer involved the motion of a chain molecule over potential energy barriers and further suggested that the yield stress is a linear function of the logarithm of the strain rate.

In another study on the effects of the strain rate, Okoli [12] carried out tensile, shear and three-point bend tests on a woven glass/epoxy laminate. A linear relationship between expended energy and the logarithm of the strain rate was indicated. This could be explained by the failure modes of the composite laminates. Since matrix yielding increased with strain rate, a greater role is played by the matrix in the fracture process and hence, more energy is expended. Results also suggested that both the shear and flexural energies to yield of the woven laminates varied linearly with the strain rate.

As noted by Taniguchi *et al*. [13], most composite materials displayed strain rate effects on mechanical properties under loading in matrix-dominant directions. In addition, the strain rate dependence of the tensile strength was higher in specimens with higher fiber orientation. Their investigations showed the carbon fiber reinforced thermoplastic epoxy specimen fractured without a necking process under dynamic loading. This contrasted with quasi-static loading, under which the necking process resulted in a large fracture strain. Higher strain rates were observed to yield larger tensile strengths as well as elastic moduli, including transverse and shear. The Poisson's ratio, on the other hand, decreased with the strain rate.

Shokrieh and Omidi [14] examined the behavior of unidirectional glass fiber reinforced polymeric composites under uniaxial loading at quasi-static and intermediate strain rates of between 0.001 and 100 $s^{-1}$. They reported that the tensile strength and the absorbed failure energy of the composites enhanced significantly with increasing strain rate. Moreover, the tensile modulus and the strain to failure both showed slight increases when strain rates are raised. Failure modes were also observed to change from quasi-static to high dynamic loading conditions.

Table 1. Review of experimental results on the effect of strain rate on the mechanical properties of composites.

| Study by | Composite | Effect of increasing strain rate on | | | |
|---|---|---|---|---|---|
| | | Ultimate tensile strength | Modulus | Failure strain | Other characteristics |
| Armenakas and Sciammarella [6] | Glass/epoxy | Decrease | Increase | Decrease | - |
| Lifshitz [7] | Angle ply glass/epoxy | Increase | Independent | Independent | - |
| Daniel *et al.* [8] | Carbon/epoxy | Independent | Increase slightly | Independent | - |
| Harding and Welsh [9] | Glass/epoxy | Increase | Increase | Increase | Absorbed failure energy increases |
| | Carbon/epoxy | Independent | Independent | - | - |
| Melin and Asp [10] | Transverse carbon/epoxy | Increase slightly | Independent | Increase slightly | - |
| Okoli and Smith [11] | Glass/epoxy | Increase | Increase | - | Poisson's ratio independent |
| Okoli [12] | Glass/epoxy | - | - | - | Absorbed failure energy increases |

| Study | Composite | Effect of increasing strain rate on | | | |
|---|---|---|---|---|---|
| | | Ultimate tensile strength | Modulus | Failure strain | Other characteristics |
| Taniguchi *et al*. [13] | Carbon/ thermoplastic epoxy | Increase slightly | Increase | Decrease | Poisson's ratio decreases |
| Shokrieh and Omidi [14] | Glass/epoxy | Increase | Increase slightly | Increase slightly | Absorbed failure energy increases |

It is noted that several of the above studies suggested linear relationships between the logarithm of strain rate and various material characteristics including dynamic elastic modulus, yield stress and expended energy.

$$E = a\log\dot{\varepsilon} + b \tag{2}$$

$$\sigma_y = c\log\dot{\varepsilon} + d \tag{3}$$

$$w = e\log\dot{\varepsilon} + f \tag{4}$$

Equations (2) and (4) demonstrate the relationships in a general form. A more useful form of the equations is presented in Equations (5) to (7).

$$\frac{E}{E_0} - 1 = k \log\left(\frac{\dot{\varepsilon}}{\dot{\varepsilon}_0}\right) \tag{5}$$

$$\frac{\sigma_y}{\sigma_{y,0}} - 1 = l \log\left(\frac{\dot{\varepsilon}}{\dot{\varepsilon}_0}\right) \tag{6}$$

$$\frac{w}{w_0} - 1 = m \log\left(\frac{\dot{\varepsilon}}{\dot{\varepsilon}_0}\right) \tag{7}$$

In these equations, the dynamic elastic modulus, the yield stress and the expended energy are normalized against corresponding reference values evaluated or determined at a reference strain rate. The reference values and the reference strain rate are denoted by the subscript '0'.

The Cowper-Symonds constitutive equation of Equation (1) may be rearranged as follows:

$$\log\left(\frac{\sigma}{\sigma_0} - 1\right) = \frac{1}{p} \log\left(\frac{\dot{\varepsilon}}{D}\right) \tag{8}$$

It may thus be seen that the main difference between Equations (6) and (8) is in the left-hand sides of the equations. In Equation (8), the logarithm of the normalized stress is taken but not in Equation (6).

Taken together, Equations (2) to (4) imply a constant yield strain as the strain rate varies, as shown below.

$$w = \frac{1}{2}\sigma_y \varepsilon_y$$

$$= \frac{1}{2}\frac{\sigma_y^2}{E}$$

$$= \frac{1}{2}\frac{\left(c\log\dot{\varepsilon} + d\right)^2}{a\log\dot{\varepsilon} + b}$$

$$= \frac{1}{2}\frac{c^2\left(\log\dot{\varepsilon}\right)^2 + 2cd\log\dot{\varepsilon} + d^2}{a\log\dot{\varepsilon} + b}$$

$$= \frac{1}{2}\left\{\frac{c^2}{a}\log\dot{\varepsilon} + \frac{2cd}{a} - \frac{bc^2}{a^2} + \frac{d^2 - \frac{2abcd - b^2c^2}{a^2}}{a\log\dot{\varepsilon} + b}\right\}$$

Thus, by comparing coefficients with Equation (4), Equations (9) to (10) may be obtained.

$$\frac{c^2}{a} = 2e \tag{9}$$

$$\frac{2cd}{a} - \frac{bc^2}{a^2} = 2f \tag{10}$$

$$d^2 - \frac{2abcd - b^2c^2}{a^2} = 0 \tag{11}$$

In particular, Equation (11) may be further manipulated to give Equation (12).

$$a^2d^2 - 2abcd + b^2c^2 = 0$$

$$\left(ad - bc\right)^2 = 0$$

$$ad = bc$$

$$d = \frac{bc}{a} \tag{12}$$

Thus,

$$\varepsilon_y = \frac{\sigma_y}{E} \quad \varepsilon_y = \frac{\sigma_y}{E}$$

$$= \frac{c\log\dot{\varepsilon} + d}{a\log\dot{\varepsilon} + b}$$

$$= \frac{c}{a} + \frac{d - \frac{bc}{a}}{a\log\dot{\varepsilon} + b}$$

$$= \frac{c}{a}$$

$$= \text{constant}$$

Thus, in materials where yield strains are not constant with varying strain rates, this may be attributed to at least one of the following reasons over the relevant range of strain rates:

(i) The elastic modulus is not a linear function of the strain rate in this material;

(ii) The yield stress is not a linear function of the strain rate in this material;

(iii) The strain energy is not a linear function of the strain rate in this material.

## B. OBJECTIVES

An objective of the current study is to examine the mechanical characteristics of a material when it is subjected to dynamic uniaxial loads. It has been noted that few studies have reported the variation of the elastic modulus with strain rate in metals. Thus, one purpose of the current study is to ascertain this relationship through tensile experiments.

With the appreciation of the dynamic loading characteristics of a material, the study seeks to establish the latter's failure envelopes in term of strain rates and normalized failure strengths. In addition, this study also investigates the failure criterion when a material is dynamically loaded to low strain rates of less than 1 $s^{-1}$. To the author's best knowledge, there has been no failure criterion proposed for a varying strain-rate loading condition.

Chapter II of this report describes the experimental setup and procedures employed in this study. Results and discussion are contained in Chapter III while Chapter IV closes with conclusion and recommendations.

THIS PAGE INTENTIONALLY LEFT BLANK

# II. EXPERIMENTAL SETUP AND PROCEDURES

The material of the specimens tested is aluminum alloy AA3003-H14. The dimensions of the specimens are given in Figure 1. The thickness of the specimens is 3.175 mm.

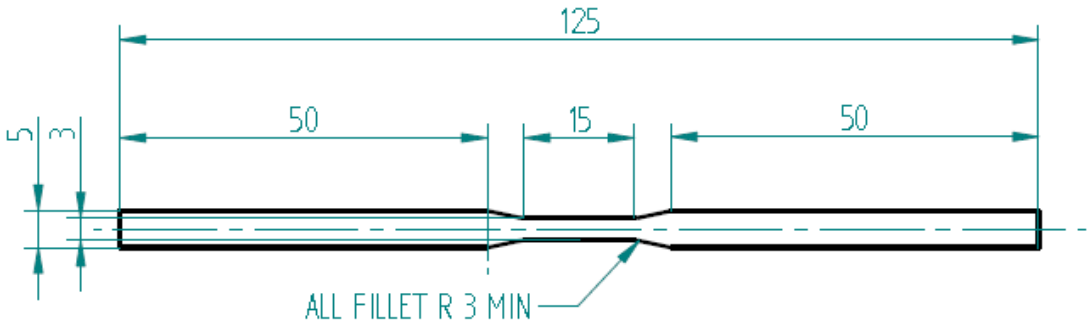


Figure 1. Dimensions of test specimens. All dimensions in millimeters.

The dimensions of the test sections of the specimens are first measured using a pair of vernier calipers. Tensile experiments are thereafter carried out on an Instron 4507 Universal Materials Testing Machine at room temperature with a 20 kN load cell. The results of the tests are retrieved using a Series IX Instron software. Two important limitations of the current experiments are a maximum crosshead speed of 500 mm/min on the testing machine and a maximum data acquisition rate of $\frac{50}{3}$ Hz. These restrict the maximum strain rate that may be tested in the experiments.

In the first set of experiments, strain rate is varied between $10^{-3}$ $s^{-1}$ and 5 x $10^{-1}$ $s^{-1}$. Strain rate may be calculated from the crosshead speed of the testing machine using Equation (13).

$$\dot{\varepsilon} = \frac{V}{l_0} \tag{13}$$

V and $l_0$ denote the crosshead speed of the testing machine and the gauge length of the specimen respectively. Thus, with a gauge length of 15 mm, crosshead speeds of 0.9 mm/min, 9 mm/min, 45 mm/min, 90 mm/min, 270 mm/min and 450 mm/min are tested. Crosshead speeds and hence, strain rates, are maintained constant throughout each test.

All experiments are repeated and consistency is verified between the two sets of data. Parameters are thereafter computed as the average of the two.

Figure 2 shows a typical stress-strain curve obtained in these experiments.

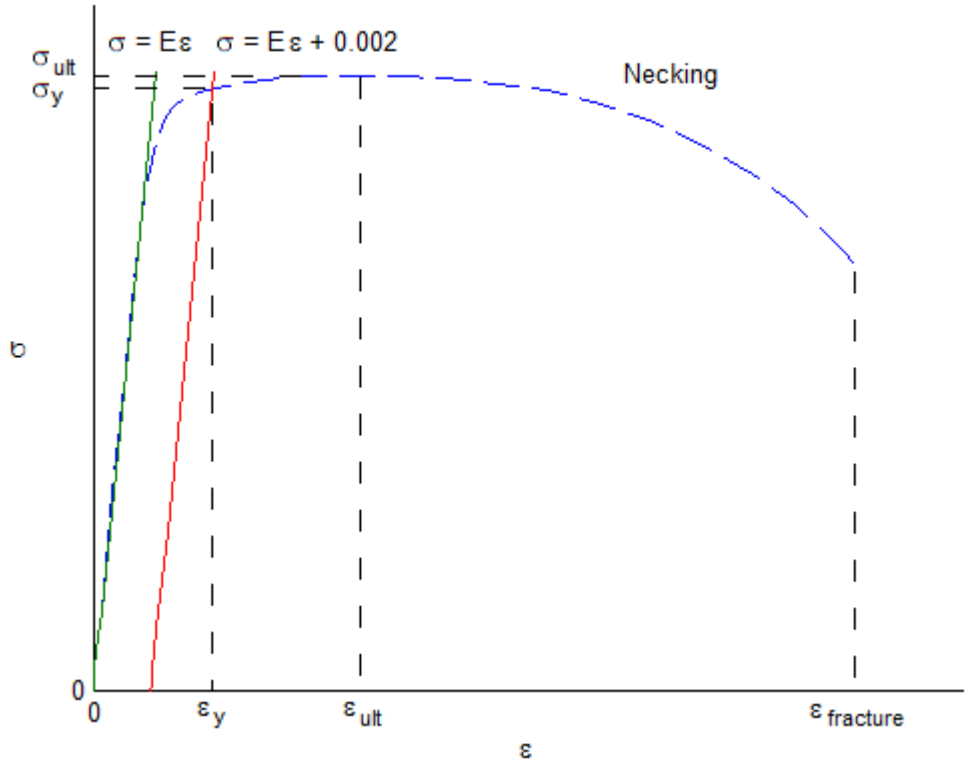


Figure 2. A typical stress-strain curve.

A straight line passing through the origin is first fitted to the linear portion of the curve. The elastic modulus is thus obtained as the slope of the straight line. In determining the yield strength and strain, the offset method is used. A second straight line

parallel to the first is offset 0.2% to the right of the latter. The 0.2% yield point is hence located where the second line interests the stress-strain curve. Numerical integration is carried out to compute the area under the curve so as to evaluate the strain energy.

In addition to the first set of experiments which are performed with constant strain rates in this study, a second set of experiments are carried out, in which the strain rate is altered in each test. More specifically, in these experiments, the test is started with an initial crosshead speed. This is kept constant before it undergoes a step change in crosshead speed to a second speed. The latter is again maintained constant until the specimen fails. Table 2 tabulates the corresponding strain rates and the strains at which the changes in strain rate occur in these experiments.

Table 2. Parameters in varying strain rate experiments.

| No. | First strain rate (1/s) | Second strain rate (1/s) | Transition strain |
|---|---|---|---|
| 1 | 0.01 | 0.30 | 0.00556 |
| 2 | 0.01 | 0.30 | 0.00592 |
| 3 | 0.01 | 0.30 | 0.01059 |
| 4 | 0.01 | 0.30 | 0.01023 |
| 5 | 0.30 | 0.01 | 0.01930 |
| 6 | 0.30 | 0.01 | 0.02132 |

These varying strain rate experiments object to examine the criterion for material ductile failure under varying strain rate loading conditions.

THIS PAGE INTENTIONALLY LEFT BLANK

# III. RESULTS AND DISCUSSION

The variations of the ultimate and yield stresses with strain rate are shown in Figure 3. Both the ultimate and yield stresses increase at higher strain rates. In addition, the rates of increase are noticeably higher at lower strain rates.

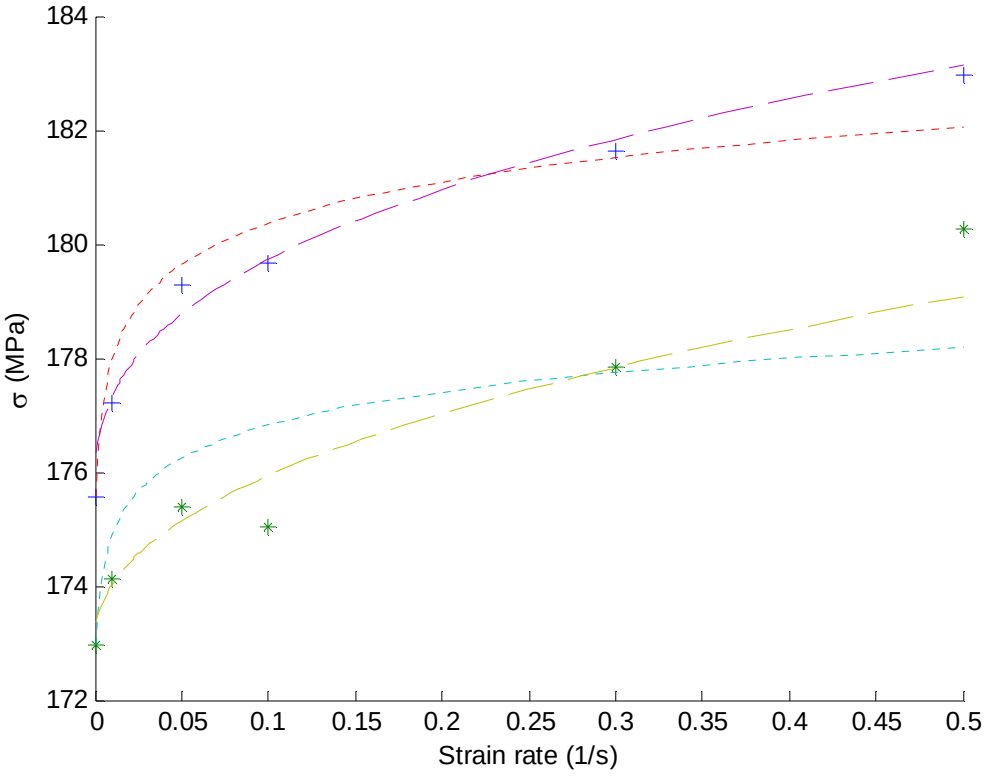


+: Ultimate strength; *: Yield strength; Dotted lines: Curves fitted to $\frac{\sigma_y}{\sigma_{y,0}} = l \log\left(\frac{\dot{\varepsilon}}{\dot{\varepsilon}_0}\right) + 1$ and $\frac{\sigma_{ult}}{\sigma_{ult,0}} = n \log\left(\frac{\dot{\varepsilon}}{\dot{\varepsilon}_0}\right) + 1$; Dashed lines: Curves fitted to $\sigma_y = \sigma_{y.0}[1 + \frac{\dot{\varepsilon}}{D_y}]^{\frac{1}{p_y}}$ and

$$\sigma_{ult} = \sigma_{ult.0}[1 + \frac{\dot{\varepsilon}}{D_{ult}}]^{\frac{1}{p_{ult}}}.$$

Figure 3. Variation of the ultimate and yield strengths with strain rate.

Experimental data is fitted both to Equations (6) and (14) as well as to Equations (15) and (16). While agreement is good with either set of equations, better agreement is found with Equations (15) and (16). In addition, a more apparent difference between the two sets of equations will be shown later.

$$\frac{\sigma_{ult}}{\sigma_{ult,0}} = n \log\left(\frac{\dot{\varepsilon}}{\dot{\varepsilon}_0}\right) + 1 \tag{14}$$

$$\sigma_y = \sigma_{y.0}[1 + \frac{\dot{\varepsilon}}{D_y}]^{\frac{1}{p_y}} \tag{15}$$

$$\sigma_{ult} = \sigma_{ult.0}[1 + \frac{\dot{\varepsilon}}{D_{ult}}]^{\frac{1}{p_{ult}}} \tag{16}$$

The coefficients, l and n, are determined as 0.0112 and 0.0137 respectively. $D_y$, $p_y$, $D_{ult}$ and $p_{ult}$ are evaluated as 885 $s^{-1}$, 2.24, 2260 $s^{-1}$ and 2.68 respectively.

The strains at yield, ultimate load and fracture show increasing trends with strain rate, as shown in Figure 4. It may be observed that the increases in fracture strain are more pronounced at strain rates of below approximately $10^{-1}$ $s^{-1}$. On the other hand, the yield strain remains relatively constant at strain rates of below approximately $10^{-1}$ $s^{-1}$ and increases thereafter with strain rate.

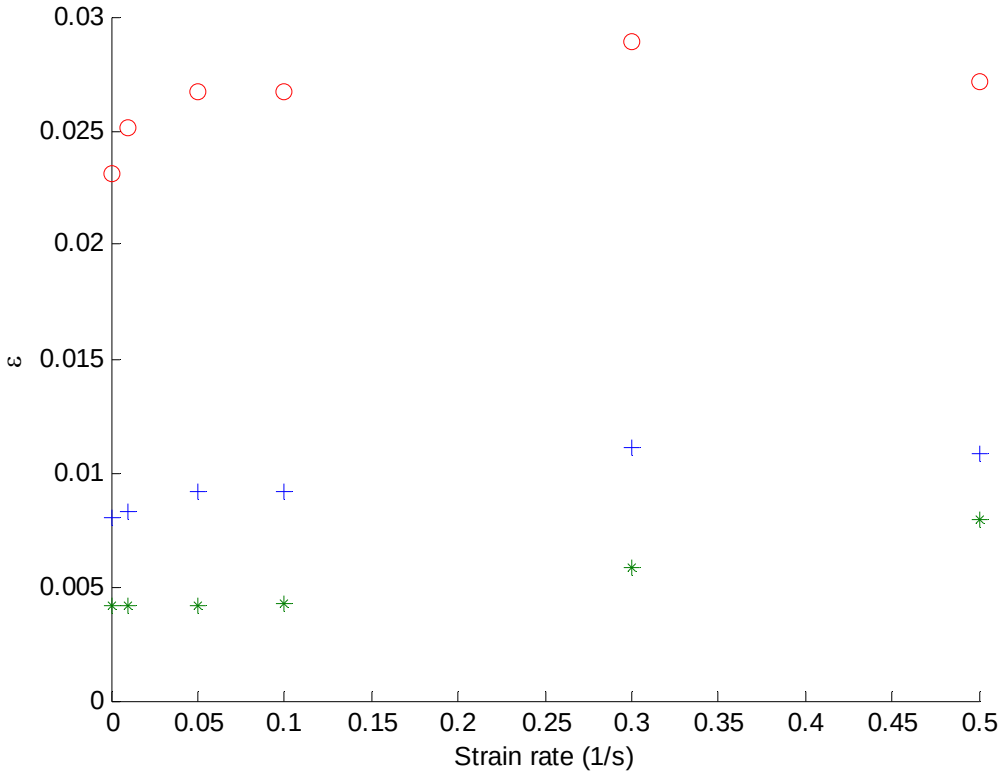


O: Strain at fracture; +: Strain at ultimate load; *: Strain at yield.

Figure 4. Variation with strain rate of the strains at fracture, ultimate load and yield.

The elastic modulus is plotted against strain rate on a logarithmic scale in Figure 5 for a better illustration of its variation with strain rate. As may be appreciated from the figure, the elastic modulus remains relatively constant at strain rates of below $10^{-1}$ $s^{-1}$. Above this strain rate, the elastic modulus follows an approximately linear negative trend with the logarithm of the strain rate.

Figures 6 and 7 plot normalized yield and ultimate stresses respectively against the inverse of the strain rate. Results from various studies are compared with results from the current study. The stresses are normalized by a corresponding reference value in the particular study. This is taken as the yield or ultimate stress obtained in the test of the lowest strain rate.

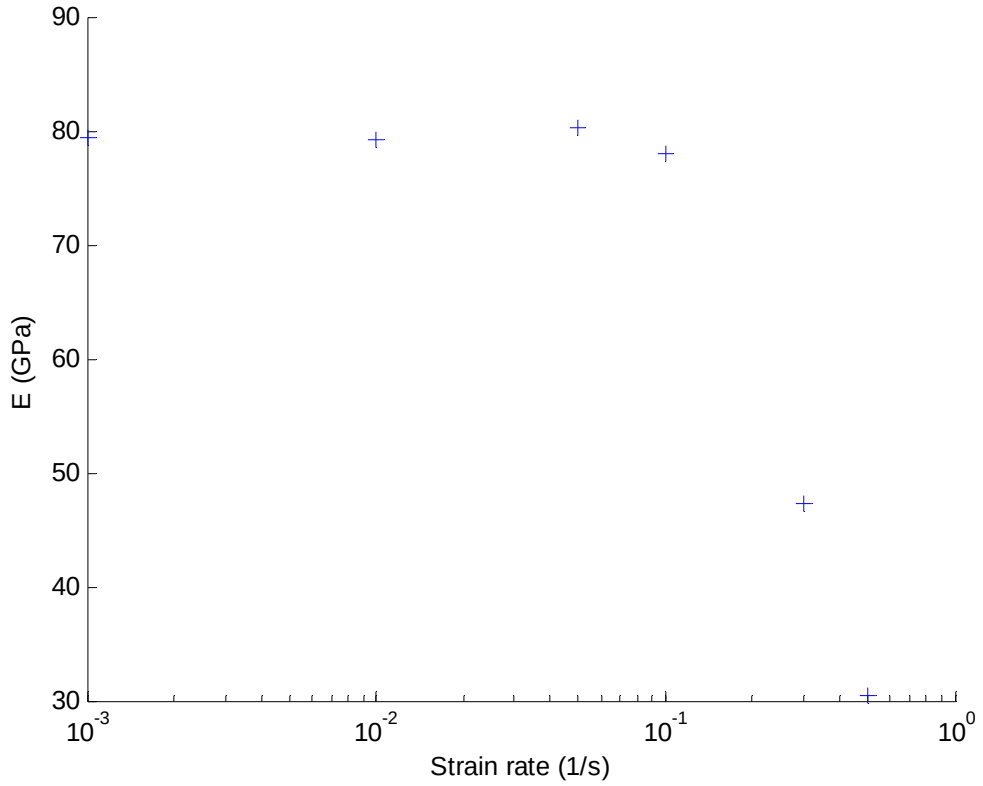


Figure 5. Variation of the elastic modulus with strain rate.

At low deformation rates, the data shows relative insensitivity of both the normalized yield and ultimate stresses to the strain rate. On the other hand, as the strain rate is increased beyond $10^{-1}$ $s^{-1}$, both the normalized yield and ultimate stresses increase noticeably.

The inverse of the strain rate, which is plotted on the x-axis in the figures, gives an indication of the duration of time that the material is allowed to deform. Plastic deformation by loading beyond the yield strength or failure at ultimate strength, respectively, occurs in the material when the stress level lies in the shaded zones above and to the right of the plotted points. The plots show that when deformation is rapid and the material is not allowed a sufficient time to deform, plastic deformation and failure in the materials are delayed to higher stresses. This effect, however, may be observed to diminish when the strain rates are less than $10^{-1}$ $s^{-1}$.

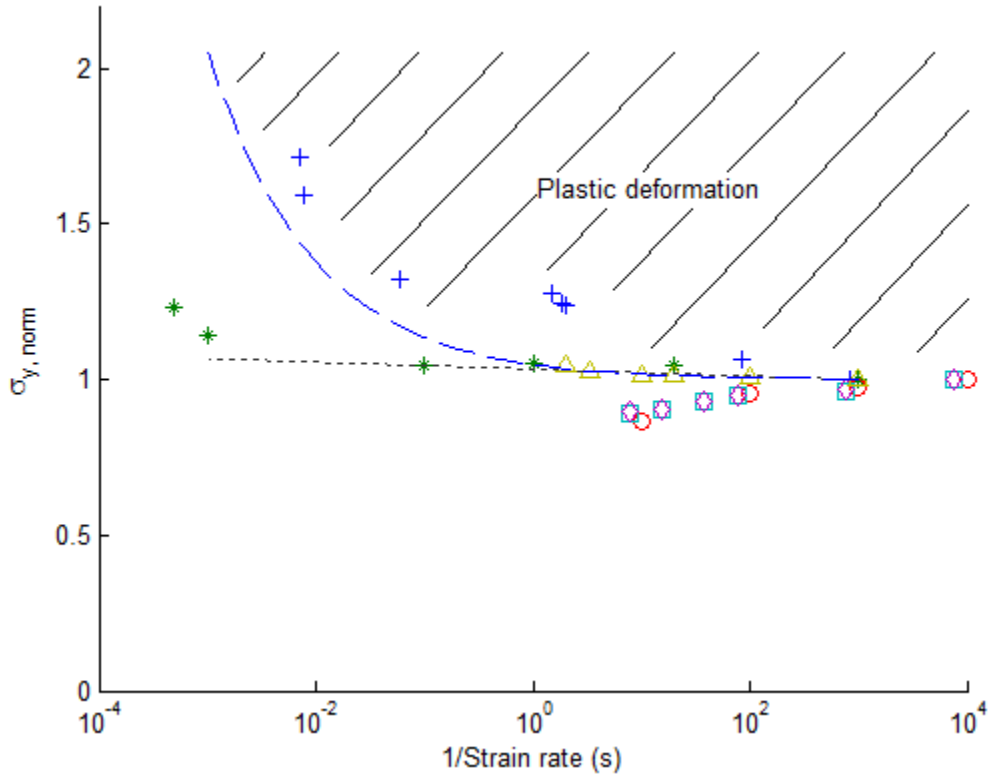


+: Yu and Jones (Mild steel) [4]; *: Mukai *et al.* (IN905XL) [2]; o: Srivatsan *et al.* (AA6061) [3]; □: Hadianfard *et al.* (AA5182) [1]; ◊: Hadianfard *et al.* (AA5754) [1]; Δ: Current study (AA3003); Dotted line: Curve fitted to $\frac{\sigma_y}{\sigma_{y,0}} = l \log\left(\frac{\dot{\varepsilon}}{\dot{\varepsilon}_0}\right) + 1$; Dashed line: Curve fitted to $\sigma_y = \sigma_{y.0}[1 + \frac{\dot{\varepsilon}}{D_y}]^{\frac{1}{p_y}}$.

Figure 6. Variation of normalized yield strength with the inverse of the strain rate.

The dotted and dashed lines in the graphs represent extrapolated curves fitted to Equations (6), (14), (15) and (16). Generally, Equations (15) and (16) are better representations of the experimental data obtained than Equations (6) and (14). The dashed lines in Figures 6 and 7 thus define envelopes for plastic deformation and failure in terms of the strain rate and the normalized yield and ultimate strengths.

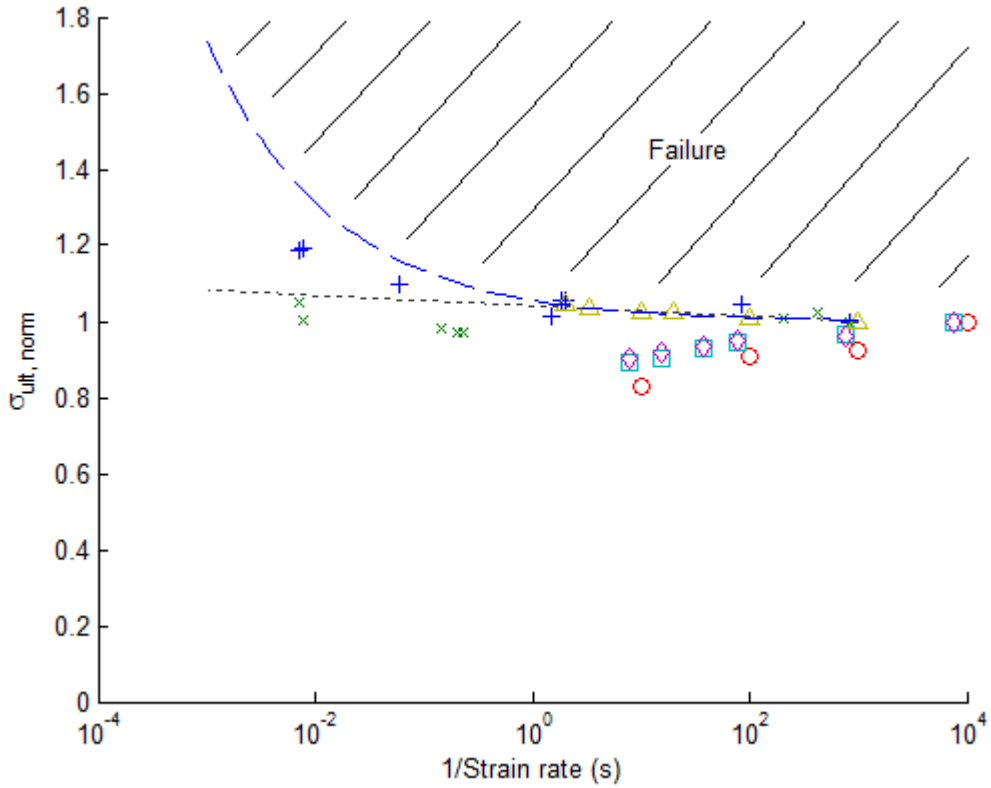


+: Yu and Jones (Mild steel) [4]; x: Yu and Jones (Aluminum alloy) [4]; o: Srivatsan *et al.* (AA6061) [3]; □: Hadianfard *et al.* (AA5182) [1]; ◊: Hadianfard *et al.* (AA5754) [1]; Δ: Current study (AA3003); Dotted line: Curve fitted to $\frac{\sigma_{ult}}{\sigma_{ult,0}} = n \log\left(\frac{\dot{\varepsilon}}{\dot{\varepsilon}_0}\right) + 1$; Dashed line: Curve fitted to $\sigma_{ult} = \sigma_{ult.0}[1 + \frac{\dot{\varepsilon}}{D_{ult}}]^{\frac{1}{p_{ult}}}$.

Figure 7. Variation of normalized ultimate strength with the inverse of the strain rate.

The total strain energy density absorbed by the material to failure is plotted as a function of strain rate in Figure 8. It is shown to increase with increasing strain rates. However, the rate of increase diminishes at higher strain rates. Equation (7) may be fitted to the experimental data with good agreement, as may be observed in Figure 8. The coefficient, m, is obtained as 0.106.

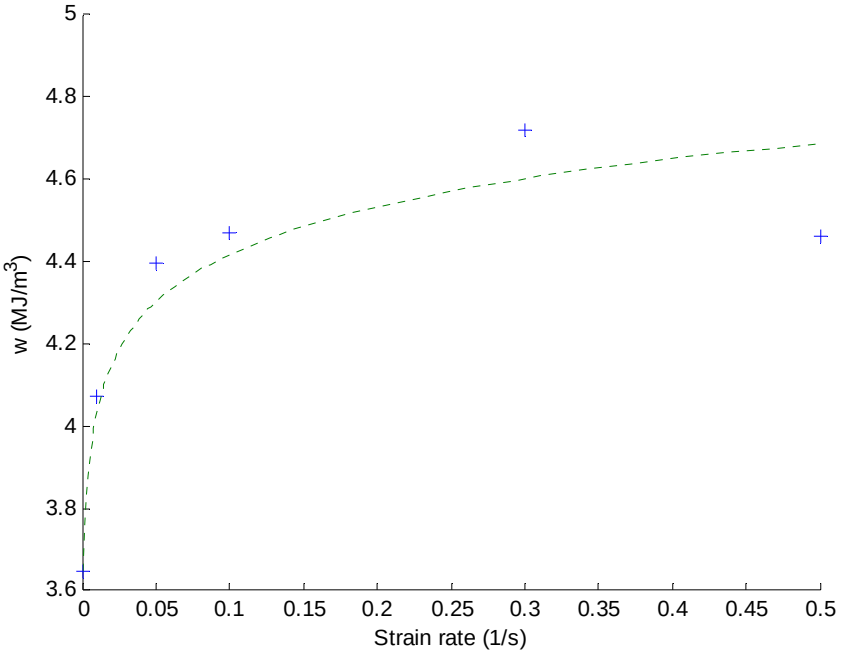


(a) Strain rate in linear scale.

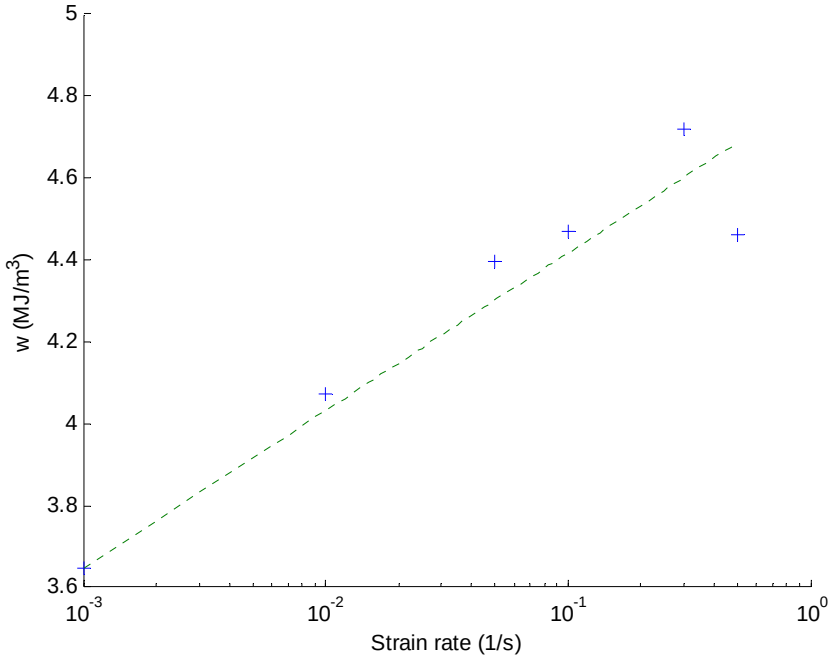


(b) Strain rate in logarithmic scale.

Figure 8. Variation of the total strain energy density with strain rate.

Total strain energy density comprises elastic and plastic strain energy densities. Figure 9 shows the effect of strain rate on the elastic strain energy density. As suggested in Figure 9, the elastic strain energy density may be expressed as a positive linear function of the strain rate. This is given in Equation (17).

$$w_e = q\dot{\varepsilon} + r \tag{17}$$

The values of q and r are 0.433 and 0.0772 respectively.

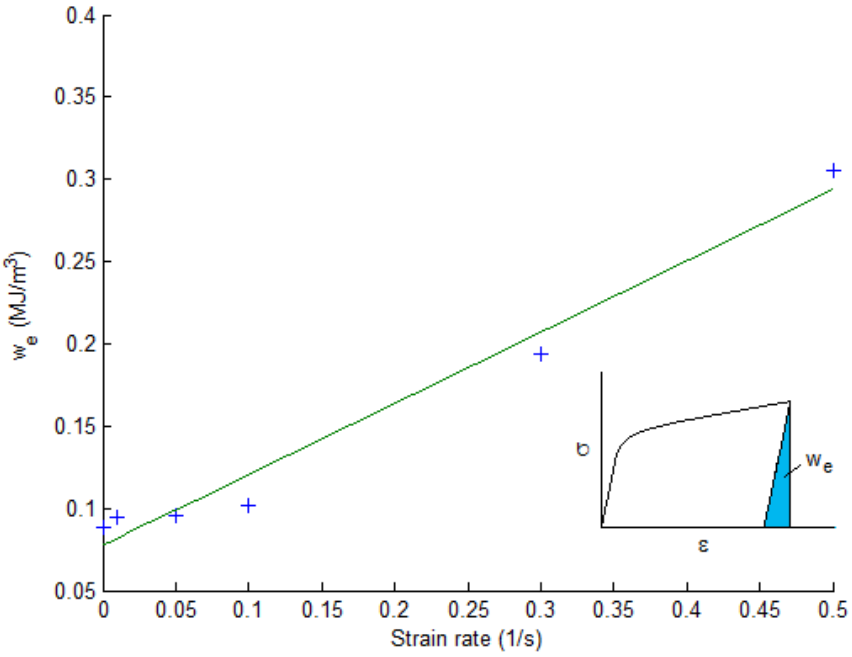


Figure 9. Variation of the elastic strain energy with strain rate. Inset shows the definition of elastic strain energy.

The variation of the plastic strain energy density with strain rate is illustrated in Figure 10. Strain rate may be observed to have a similar effect on the plastic strain energy density as the total strain energy. The plastic strain energy density increases as the strain

rate increases. However, the rate of increase diminishes at higher strain rates. When Equation (18) is fitted to the experimental data, reasonable agreement is found with the coefficient, s, evaluated as 0.0966.

$$\frac{w_p}{w_{p,0}} - 1 = s \log\left(\frac{\dot{\varepsilon}}{\dot{\varepsilon}_0}\right) \tag{18}$$

It is noted, however, that Equation (18) does not reconcile with Equations (7) and (17). This may be explained in the following.

$$w = w_e + w_p$$

$$w_p = w - w_e \tag{19}$$

Equation (18) may be used to evaluate the left hand side of Equation (19) as below.

$$\text{LHS of Equation (19)} = w_{p,0} s \log\left(\frac{\dot{\varepsilon}}{\dot{\varepsilon}_0}\right) + w_{p,0}$$

$$= s' \log\left(\frac{\dot{\varepsilon}}{\dot{\varepsilon}_0}\right) + w_{p.0} \text{ where } s' = w_{p,0} s \tag{20}$$

On the other hand, when the right hand side of Equation (19) is evaluated with Equations (7) and (17), another expression for the plastic strain energy may be obtained.

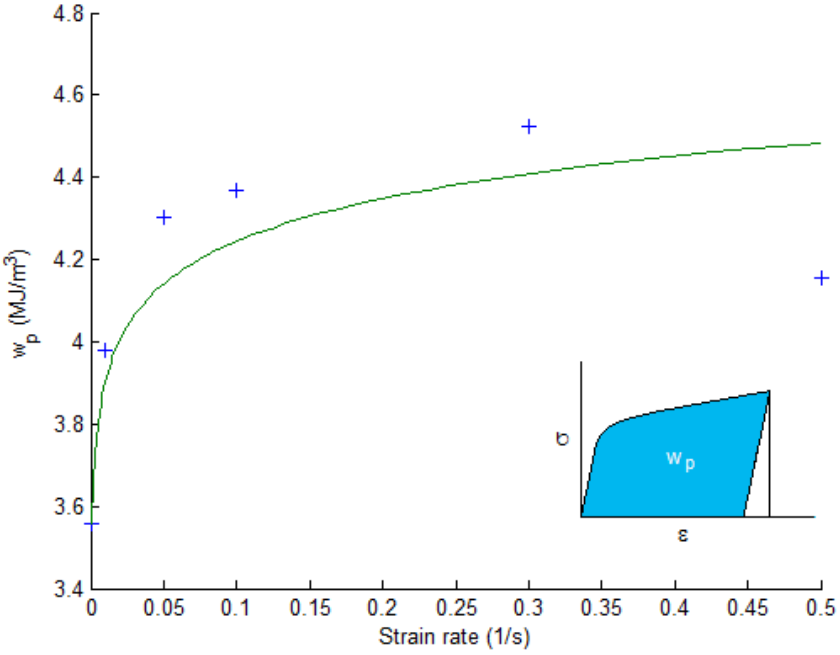


(a) Strain rate in linear scale.

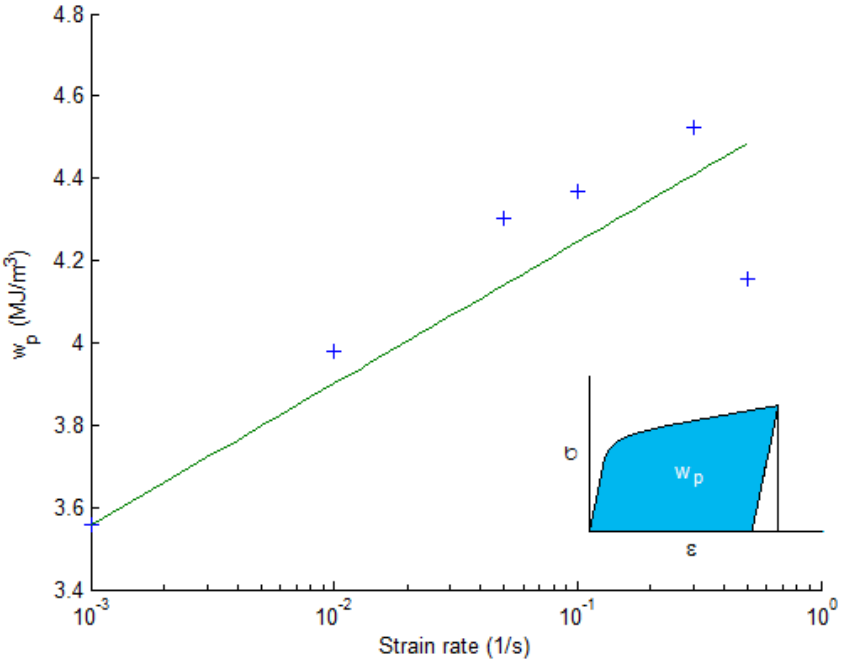


(b) Strain rate in logarithmic scale.

Figure 10. Variation of the plastic strain energy with strain rate. Insets show the definition of plastic strain energy.

$$\text{RHS of Equation (19)} = w_0 m \log\left(\frac{\dot{\varepsilon}}{\dot{\varepsilon}_0}\right) + w_0 - q\dot{\varepsilon} - r$$

$$= m' \log\left(\frac{\dot{\varepsilon}}{\dot{\varepsilon}_0}\right) + w_0 - q\dot{\varepsilon} + q\dot{\varepsilon}_0 - w_{e,0} \quad \text{where } m' = w_0 m$$

$$= m' \log\left(\frac{\dot{\varepsilon}}{\dot{\varepsilon}_0}\right) + w_{p,0} - q(\dot{\varepsilon} - \dot{\varepsilon}_0)) \tag{21}$$

The difference between the above two expressions of the plastic strain energy density, that is, the difference between the left and right hand sides of Equation (19), lies in the last term of the right hand side, $-q(\dot{\varepsilon} - \dot{\varepsilon}_0)$. Due to setup limitations on the achievable range of strain rates, however, insufficient data is available in this study to resolve with confidence the validity of either expression.

As a failure criterion in ductile materials, the use of a critical value of the plastic strain energy density is appropriate. Consider, for example, a metal repeatedly loaded to different stresses below the ultimate strength and unloaded thereafter. While elastic strain energy is recovered upon each unloading, the plastic strain energy represents a reduction in the strength of the material. Material failure occurs when its plastic strain energy density exceeds a critical value. In more general terms, Li [15] concluded that material ductile failure is influenced by two dissipative mechanisms, namely, the plastic deformation dissipation and the damage dissipation.

In order to demonstrate the application of critical values of the plastic strain energy density as a ductile failure criterion, consider a general strain time history in Figure 11. In this strain time history, loading and unloading occurs at varying strain rates. However, for simplification, strain rate is discretized such that the strain rate of each

loading and unloading phase is approximated by the slope of a straight line drawn from the point of the lowest strain to the point of the highest strain. This is illustrated in Figure 11.

In this example, consider a sequential strain rate loading such as $\dot{\varepsilon}_1 = \frac{\varepsilon_1}{t_1}$, $\dot{\varepsilon}_2 = -\frac{\varepsilon_2 - \varepsilon_1}{t_2 - t_1} = \frac{\varepsilon_3 - \varepsilon_2}{t_3 - t_2} = -\frac{\varepsilon_6 - \varepsilon_5}{t_6 - t_5}$, $\dot{\varepsilon}_3 = -\frac{\varepsilon_4 - \varepsilon_3}{t_4 - t_3} = \frac{\varepsilon_5 - \varepsilon_4}{t_5 - t_4} = \frac{\varepsilon_7 - \varepsilon_6}{t_7 - t_6}$ and $\dot{\varepsilon}_4 = \frac{\varepsilon_8 - \varepsilon_7}{t_8 - t_7}$ where $\dot{\varepsilon}_1 > \dot{\varepsilon}_3 > \dot{\varepsilon}_2 > \dot{\varepsilon}_4$. The time variation of these strain rates are plotted in Figure 12.

Figure 13 shows the corresponding stress-strain curves due to the respective strain rates of $\dot{\varepsilon}_1$, $\dot{\varepsilon}_2$, $\dot{\varepsilon}_3$ and $\dot{\varepsilon}_4$. These may be determined using Equation (1) from the static stress-strain relation once the material constants are known. The variations of the stress and strain in the material with time resulting from the strain time history shown in Figure 11 is illustrated in Figure 13 in blue.

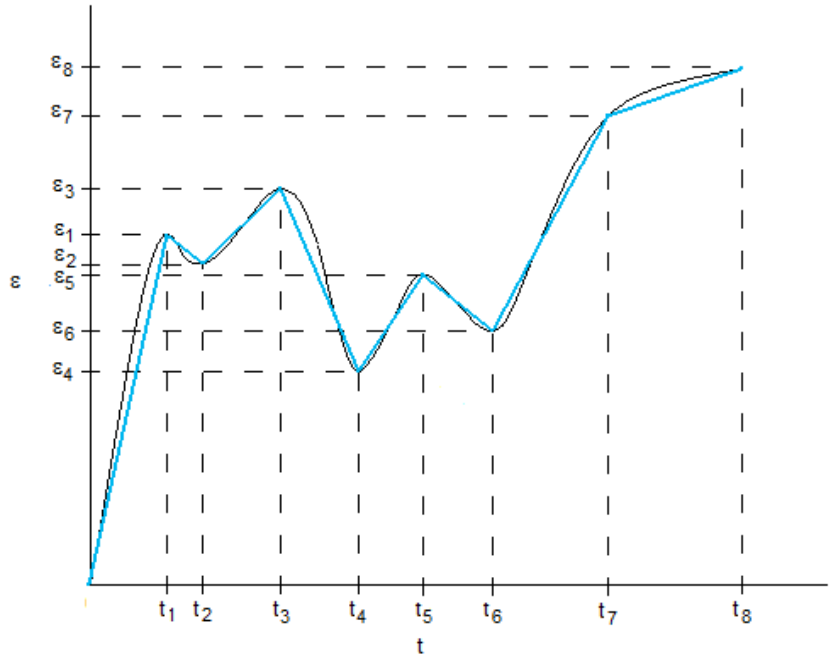


Figure 11. General strain-time history.

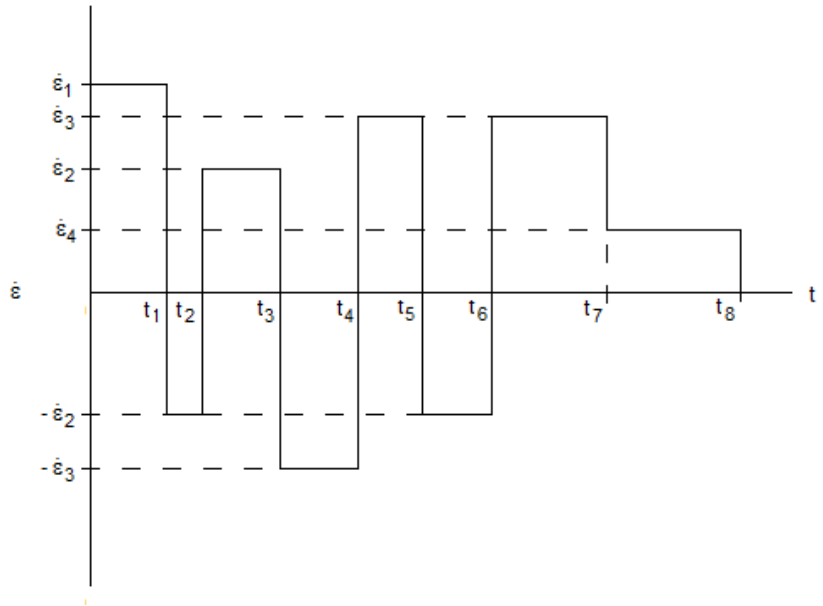


Figure 12. Time variation of strain rate due to strain time history.

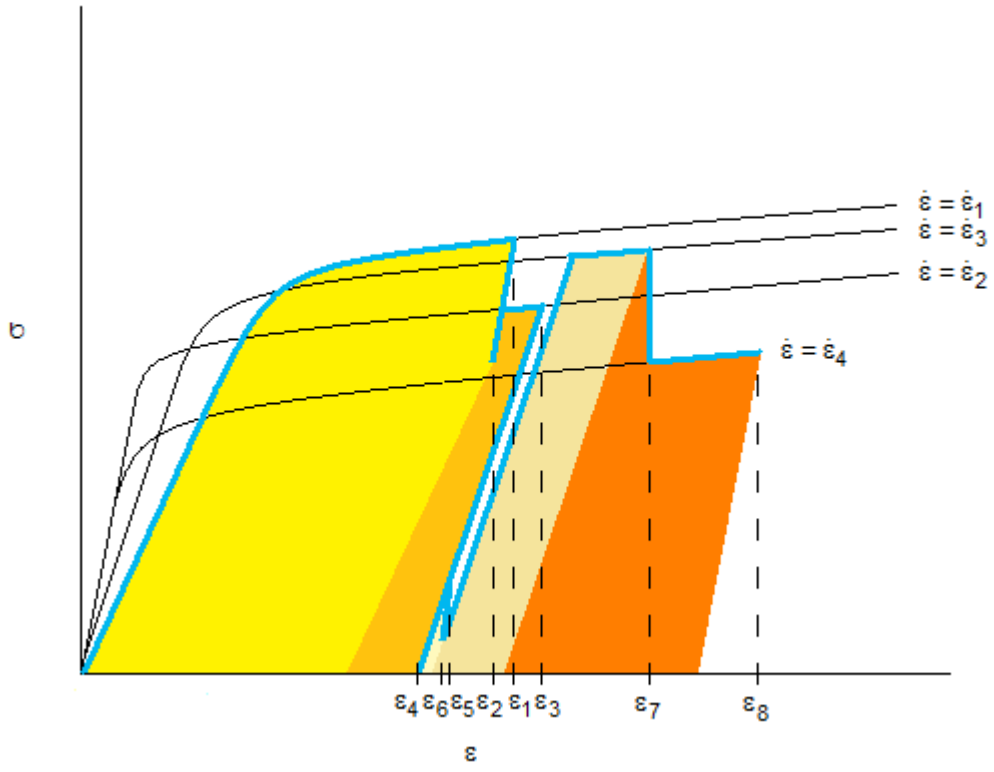


Figure 13. Stress-strain curves due to strain time history.

In each loading cycle in which the material is loaded and subsequently unloaded, its plastic strain energy gained in that loading cycle is determined as the respective shaded area. In the computation of the plastic strain energy density, it is important to note that yield strain and elastic modulus are functions of strain rate. The plastic strain energy accumulates over the loading cycles and material failure is predicted when this energy density exceeds a critical value. In particular, a failure criterion for varying strain rate dynamic loading conditions is proposed in Equation (22).

$$\sum \frac{\left(w_p\right)_i}{\left(w_{p,critical}\right)_i} = \frac{\left(w_p\right)_1}{\left(w_{p,critical}\right)_1} + \frac{\left(w_p\right)_2}{\left(w_{p,critical}\right)_2} + \ldots + \frac{\left(w_p\right)_n}{\left(w_{p,critical}\right)_n} = 1 \qquad (22)$$

$\left(w_p\right)_i$ denotes the amount of plastic strain energy density stored in the material during the *i*th loading cycle while $\left(w_{p,critical}\right)_i$ refers to the critical plastic strain energy density at the same strain rate of the loading cycle. With the discretization of the strain rate, each loading phase is deemed as occurring with a constant strain rate. Hence, the critical plastic strain energy density is a function of the strain rate of the loading phase and may be given either by Equation (20) or Equation (21).

The proposed failure criterion expressed in Equation (22) is corroborated by results obtained in the varying strain rate experiments. Figure 14 shows a typical stress-strain curve obtained in such an experiment. In this instance, the strain rate is increased from $10^{-2}$ $s^{-1}$ in the first stage of the experiment to 3 x $10^{-1}$ $s^{-1}$ in the second stage at a transition strain of 0.01023. The stress-strain curves due to the tensile tests of constant strain rates of $10^{-2}$ $s^{-1}$ and 3 x $10^{-1}$ $s^{-1}$ are shown in Figure 14 for comparison. As expected, the stress-strain curve follows that of the $10^{-2}$ $s^{-1}$ strain rate initially. Upon the step increase in strain rate to 3 x $10^{-1}$ $s^{-1}$, the stress-strain curve begins to deviate from that of the $10^{-2}$ $s^{-1}$ strain rate to lie in between the two stress-strain curves of constant strain rate.

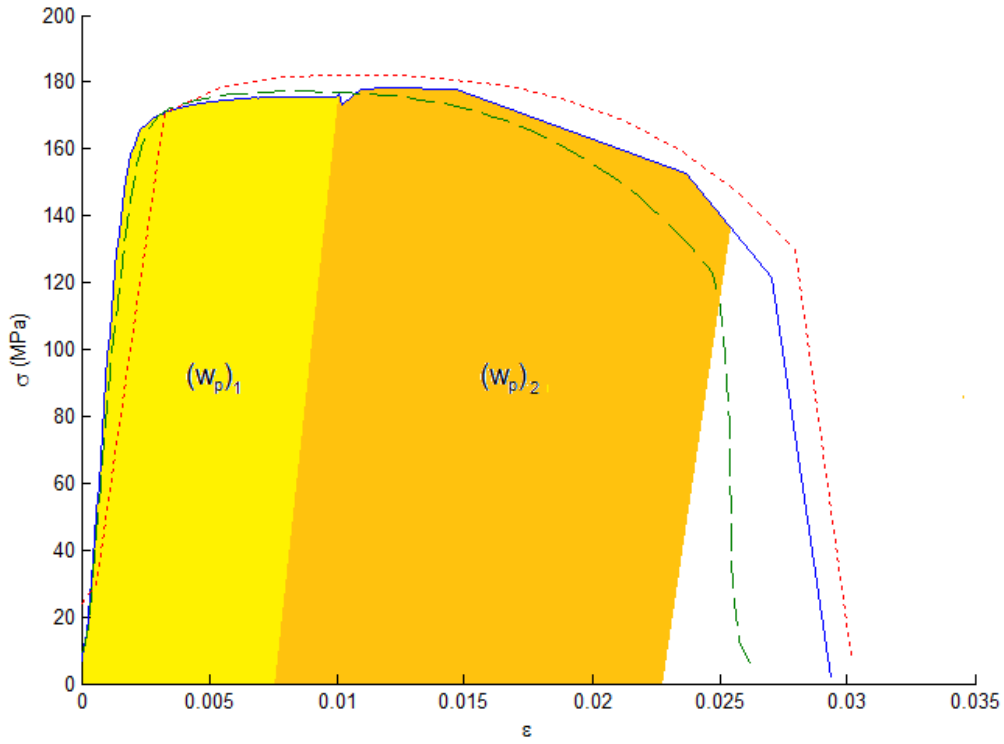


Figure 14. A typical stress-strain curve obtained in varying strain rate experiment.

In efforts to assess the validity of the proposed failure criterion, the plastic strain energy densities absorbed by the material during the two stages of each varying strain rate test, $\left(w_p\right)_1$ and $\left(w_p\right)_2$, are computed. These are determined as the shaded areas as illustrated in Figure 14 using numerical integration. Each stored plastic strain energy density is divided by its respective critical plastic strain energy density, and the two ratios are summed. Results are tabulated in Table 3, which shows that the proposed failure criterion in Equation (22) is validated by these experimental results within an error of approximately 10%.

In another approach, the proposed failure criterion is applied to each of the varying strain rate experiments to predict fracture strain. These values are estimated based on the transition strain as well as the constant strain rate stress-strain curves of the first and second strain rates. It is not presumed that stress and strain measurements are

made in the varying strain rate experiments. Table 4 compares the computed results with the empirical data, and this comparison indicates that the former approximates the latter within errors of approximately 4%.

Table 3. Results from varying strain rate experiments.

| No. | First strain rate (1/s) | Second strain rate (1/s) | Transition strain | $\left(w_p\right)_1$ (MJ/m$^3$) | $\left(w_p\right)_2$ (MJ/m$^3$) | $\sum \frac{\left(w_p\right)_i}{\left(w_{p,critical}\right)_i}$ |
|---|---|---|---|---|---|---|
| 1 | 0.01 | 0.30 | 0.00556 | 0.5482 | 3.6273 | 0.9461 |
| 2 | 0.01 | 0.30 | 0.00592 | 0.6540 | 3.5238 | 0.9501 |
| 3 | 0.01 | 0.30 | 0.01059 | 1.4644 | 2.8404 | 1.0057 |
| 4 | 0.01 | 0.30 | 0.01023 | 1.4130 | 2.7365 | 0.9695 |
| 5 | 0.30 | 0.01 | 0.01930 | 2.7684 | 1.1901 | 0.9196 |
| 6 | 0.30 | 0.01 | 0.02132 | 3.3526 | 0.6405 | 0.9086 |

Table 4. Actual and predicted fracture strains in varying strain rate experiments.

| No. | First strain rate (1/s) | Second strain rate (1/s) | Transition strain | Actual fracture strain | Predicted fracture strain | Percentage difference (%) |
|---|---|---|---|---|---|---|
| 1 | 0.01 | 0.30 | 0.00556 | 0.0270 | 0.0279 | 3.1681 |
| 2 | 0.01 | 0.30 | 0.00592 | 0.0268 | 0.0278 | 3.7789 |
| 3 | 0.01 | 0.30 | 0.01059 | 0.0279 | 0.0272 | -2.5958 |
| 4 | 0.01 | 0.30 | 0.01023 | 0.0268 | 0.0272 | 1.6833 |
| 5 | 0.30 | 0.01 | 0.01930 | 0.0274 | 0.0268 | -2.1726 |
| 6 | 0.30 | 0.01 | 0.02132 | 0.0262 | 0.0269 | 2.6252 |

More specifically, the approximation methodology is described in the following. Firstly, the stress-strain curve for the constant strain rate of the first stage is integrated from zero to the transition strain so as to obtain the plastic strain energy density gained during the first stage. $\frac{\left(w_p\right)_1}{\left(w_{p,critical}\right)_1}$ is thereby checked to be less than unity. Subsequently, the stress-strain curve for the constant strain rate of the second stage is integrated from the transition strain to an upper limit that is continually increased until the failure criterion is satisfied. The fracture strain is thus estimated by the upper limit.

In the case of the last two experiments in Table 4, when the stress-strain curve for the constant strain rate of the second stage is integrated from the transition strain to its fracture strain, $\frac{\left(w_p\right)_1}{\left(w_{p,critical}\right)_1}+\frac{\left(w_p\right)_2}{\left(w_{p,critical}\right)_2}$ remains less than unity. Thus, in order to be able to predict the fracture strain, a fourth order polynomial is fitted to the plastic deformation regime of the strain-strain curve for the constant strain rate of $10^{-1}$ $s^{-1}$ and extrapolated. This allows integration to be carried beyond the fracture strain due to the constant strain rate of $10^{-1}$ $s^{-1}$.

Additional experiments tend to suggest that the strain rate of unloading influences the variation of stress with strain during an unloading. When a material is unloaded at a particular strain rate, its stress varies as a linear function of strain. The slope of this function is perceived to be the same as the elastic modulus of that strain rate. Thus, if a material is loaded at a different strain rate than when it is unloaded, the slope during elastic deformation would differ from the slope during unloading.

The range of the strain rates tested in this study spans two different regimes. The quasi-static and dynamic regimes are classified, respectively, with strain rates of less than and more than $10^{-1}$ $s^{-1}$. This is similar to observations by Hadianfard *et al.* [1] who also differentiated between tensile tests at strain rates of less than and more than $10^{-1}$ $s^{-1}$. In the current study, differences between the two regimes are evident in Figures 4 to 7.

There are two limitations in the above result analysis. Firstly, due to a lack of data on true stress and strain, numerical integration of the area under the engineering stress-strain curve is carried out for the computation of strain energy density. Secondly, due to constraints on the maximum rate of data acquisition, the number of data points acquired in the tests of the highest strain rate is small. In particular, this reduces the accuracy of the calculated elastic modulus, yield stress and yield strain in the tests of strain rate 5 x $10^{-1}$ $s^{-1}$.

For completeness, Figure 14 is presented as the corresponding graph to Figure 7 in composite materials. Similar trends may be observed. When deformation is rapid and the material is not allowed a sufficient time to deform, material damage is delayed to higher loads. This effect, however, may be observed to diminish at strain rates of more than $10^{-1}$ $s^{-1}$.

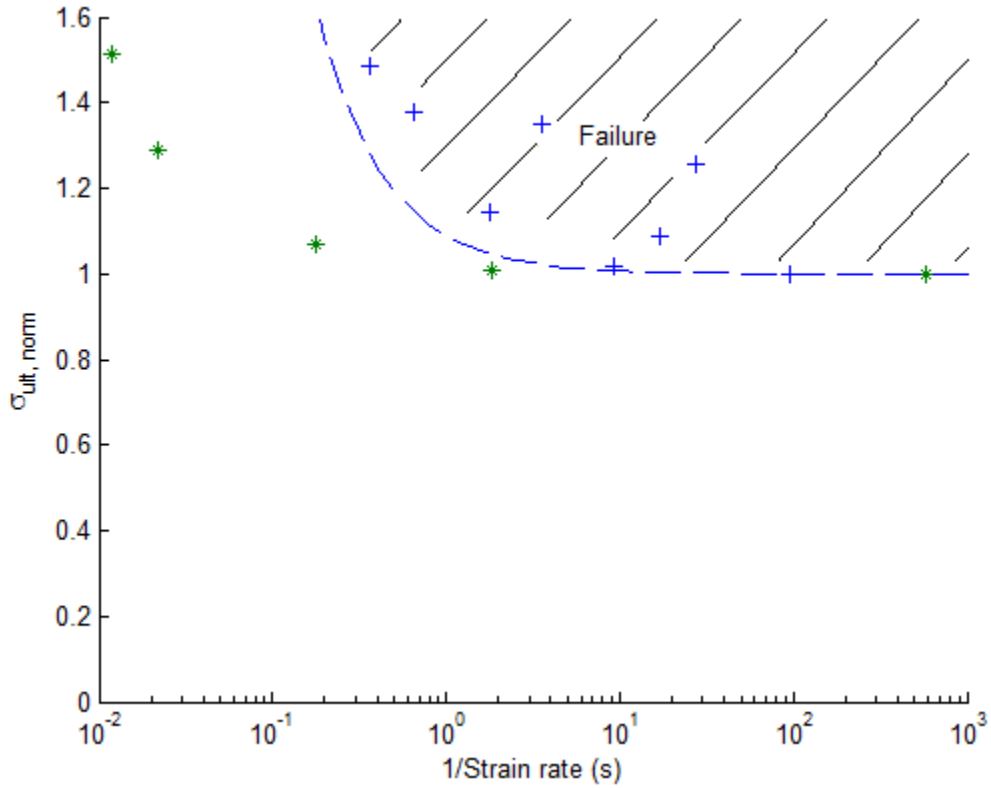


+: Okoli and Smith (Glass/epoxy) [11]; *: Shokrieh and Omidi (Glass/epoxy) [14].

Figure 15. Normalized ultimate strength as a function of the inverse of the strain rate.

# IV. CONCLUSIONS AND RECOMMENDATIONS

In conclusion, the mechanical characteristics of aluminum alloy AA3003-H14 were examined under a dynamic uniaxial loading. Both ultimate and yield strengths, as well as the absorbed strain energy density, show positive sensitivity to strain rate. Moreover, the strains at yield, ultimate load and fracture increase with strain rate. Under quasi-static strain rates of less than $10^{-1}$ $s^{-1}$, the low loading rate does not have a significant effect on the elastic modulus, the normalized yield stress or ultimate stress. On the other hand, when the material is subjected to dynamic loading rates of more than $10^{-1}$ $s^{-1}$, the elastic modulus diminishes as the strain rate increases, while both normalized yield and ultimate stresses increase noticeably. It was also noted that the amount of plastic strain energy density accumulated in a ductile material in its loading time history was useful as a failure criterion for the prediction of failure. As a result, a failure criterion was proposed for loading with varying strain rates using the concept of accumulated plastic strain energy density. The proposed criterion was validated from experiments consisting of two different strain rates applied one after another subsequently.

The current work may be extended in the following ways:

(i) The range of strain rates used in the tensile experiments may be increased. This would enable the verification of the trends observed in the current study beyond the present maximum strain rate. In particular, this would allow the resolution of an empirical expression for the plastic strain energy.

(ii) Different metals may be investigated and tested. By studying the results due to different metals, the variations of the normalized yield and ultimate stresses with the inverse of the strain rate may be compared. Their similarity or differences may thus be established.

(iii) Composite materials may be investigated and tested. Where composites fail in a brittle manner, the effects of strain rate on their mechanical properties may differ. Moreover, a different failure criterion may apply.

(iv) Much remains unclear about the behavior of materials under dynamic loading and unloading conditions of varying strain rates. More experiments designed to investigate the variation of stress with strain under these conditions would enhance the understanding of the influence of varying strain rate on the evolution of plastic strain energy.

# LIST OF REFERENCES


[1] M. J. Hadianfard, R. Smerd, S. Winkler, and M. Worswick, "Effects of strain rate on mechanical properties and failure mechanism of structural Al-Mg alloys," *Materials Science and Engineering A,* vol. 492, pp. 283–292, Sep 2008.

[2] T. Mukai, K. Ishikawa, and K. Higashi, "Influence of strain rate on the mechanical properties in fine-grained aluminum alloys," *Materials Science and Engineering A*, vol. 204, pp. 12–18, Dec 1995.

[3] T. S. Srivatsan, T. Hoff, S. Sriram, and A. Prakash, "The effect of strain rate on flow stress, strength and ductility of an Al-Li-Mg alloy," *Journal of Materials Science Letters*, vol. 9, pp. 297–300, Mar 1990.

[4] J. Yu, and N. Jones, "Further experimental investigations on the failure of clamped beams under impact loads," *International Journal of Solids and Structures*, vol. 27, no. 9, pp. 1113–1137, 1991.

[5] C. Albertini, and M. Montagnani, "Dynamic uniaxial and biaxial stress-strain relationships for austenitic stainless steels," *Nuclear Engineering and Design*, vol. 57, pp. 107–123, Apr 1980.

[6] A. E. Armenakas, and C. A. Sciammarella, "Response of glass-fiber-reinforced epoxy specimens to high rates of tensile loading," *Experimental Mechanics*, vol. 13, no. 10, pp. 433–440, Oct 1973.

[7] J. M. Lifshitz, "Impact strength of angle ply fiber reinforced materials," *Journal of Composite Materials*, vol. 10, pp. 92–101, Jan 1976.

[8] I. M. Daniel, R. H. LaBedz, and T. Liber, "New method for testing composites at very high strain rates," *Experimental Mechanics*, vol. 21, no. 2, pp. 71–77, Feb 1981.

[9] J. Harding, and L. M. Welsh, "A tensile testing technique for fibre-reinforced composites at impact rates of strain," *Journal of Materials Science*, vol. 18, pp. 1810–1826, Jun 1983.

[10] L. G. Melin, and L. E. Asp, "Effects of strain rate on transverse tension properties of a carbon/epoxy composite: studied by moiré photography," *Composites: Part A*, vol. 30, pp. 305–316, Mar 1999.

[11] O. I. Okoli, and G. F. Smith, "The effect of strain rate and fibre content on the Poisson's ratio of glass/epoxy composites," *Composite Structures*, vol. 48, pp. 157–161, Jan 2000.

[12] O. I. Okoli, “The effects of strain rate and failure modes on the failure energy of fibre reinforced composites,” *Composite Structures*, vol. 54, pp. 299–303, Nov 2001.

[13] N. Taniguchi, T. Nishiwaki, N. Hirayama, H. Nishida, H. Kawada, “Dynamic tensile properties of carbon fiber composite based on thermoplastic epoxy resin loaded in matrix-dominated directions,” *Composites Science and Technology*, vol. 69, pp. 207–213, Feb 2009.

[14] M. M. Shokrieh, and M. J. Omidi, “Tension behaviour of unidirectional glass/epoxy composites under different strain rates,” *Composite Structures*, vol. 88, pp. 595–601, Mar 2009.

[15] Q. M. Li, “Strain energy density failure criterion,” *International Journal of Solids and Structures*, vol. 38, pp. 6997–7013, Sep 2001.

# INITIAL DISTRIBUTION LIST

1. Defense Technical Information Center
   Ft. Belvoir, Virginia

2. Dudley Knox Library
   Naval Postgraduate School
   Monterey, California

3. Young W. Kwon
   Naval Postgraduate School
   Monterey, California

4. Jarema M. Didoszak
   Naval Postgraduate School
   Monterey, California

5. Kian Sing Tan
   Singapore Technologies Aerospace
   Singapore

6. Tat Soon Yeo
   Temasek Defence Systems Institute, National University of Singapore
   Singapore

7. Lai Poh Tan
   Temasek Defence Systems Institute, National University of Singapore
   Singapore